4-1-2009

Optical properties of multilayer-polyelectrolyte films with incorporated gold nanomaterials (solid nanoparticles and hollow nanoshells)

Robert Watson Day

Follow this and additional works at: http://scholarship.richmond.edu/honors-theses

Optical Properties of Multilayer-Polyelectrolyte Films with Incorporated Gold Nanomaterials (Solid Nanoparticles and Hollow Nanoshells)

by

Robert Watson Day

Honors Thesis
in
The Department of Chemistry
University of Richmond
Richmond, VA

4/24/2009

APPROVED BY:

ADVISOR

Dr. Michael Leopold
Department of Chemistry
University of Richmond

SECOND READER

Dr. Will Case
Department of Chemistry
University of Richmond

<u>Dedication</u>

I would like to dedicate this thesis to my parents for their continual support; my research advisor, Dr. Michael Leopold for his invaluable guidance; and Anna Parker for always being encouraging and inquisitive.

Table of Contents

Acknowledgements

Abstract

The growth of various multilayer-polymer multilayer-nanoparticle films was successfully achieved. Multilayer-polymer multilayer-nanoparticle films with 1, 3, and 5 polymer layers between nanoparticle layers exhibit significantly different optical properties due to the differences in magnitude of particle plasmon coupling. These film systems were also successfully extended to hollow gold nanoshells, which have significantly enhanced optical properties in comparison to solid gold nanoparticles of similar sizes. A proposal for utilizing this increased sensitivity of the gold nanoshells to explore the 'microenvironments' for optimizing potential sensing applications is also presented.

Background

Nanoscience[1,2] is a rapidly expanding area with sub-divisions in many traditional fields of study (e.g. chemistry, physics, materials science, surface science, electronics, optics, etc.) and has frequently served as a bridge between various inter-disciplinary investigations. Much is still unknown about the capabilities and fundamental limits of nanomaterials for improving technologies since this scale range has traditionally been given less attention than either macroscopic objects, or individual atoms and molecules[3,6]. Some, however, including Murray et al,[4,5] have been actively exploring gold nanoparticles/nanoclusters with regard to both sides of the "nanospectrum": (1) what marks the division between molecules and nanoparticles?; similarly, (2) what marks the division between nanoparticles and bulk materials?; and (3) how can these properties which are inherently unique to materials at the nanoscale be utilized to improve current devices or to develop completely novel technologies?

These nanomaterials can be composed of a wide variety of matter as well. Various carbon nanomaterials[7,8] are actively being pursued including C_{60}, carbon nanotubes, and graphene. Silicon is being explored in nanoparticle form as efficient scaffolds for drug delivery or for protective coatings at the nanoscale, and silicon nanowires[9] are being investigated for renewable energy applications. The noble metals (e.g. gold, silver, etc.) are another class of material which are of interest to materials science because they are highly resistant to corrosion, oxidation, and many other common reactions.[10,11] They also have certain unique optical properties that only exist when their dimensions lie on the nanoscale.

One of the reasons that nanomaterials are currently of significant interest is the etymologically obvious one (i.e. their small size). Indeed, most physical interactions between two substances are determined solely by the nature of the surface. As the dimensions of a

spherical material (radius = r) decrease, for example, its volume ($V \alpha r^3$) decreases at a much greater rate than its surface area ($SA \alpha r^2$). Therefore, materials in the nanoscale have high surface area to volume ratios - a characteristic which is important for catalysis, increasing the efficiency for various processes, decreasing the need, and thus cost, for a given material, as well as decreasing waste, which might be detrimental to the environment or cause health problems. A second main reason for interest is the fact that much of nature's biological machinery (e.g. proteins, DNA, mitochondria, etc.) exists on the nanoscale – a characteristic that could be exploited for improving the understanding of biology through size-optimized experiments, and for enhancing a wide array of medical techniques (e.g. cancer detection/therapy, imaging, drug delivery). In addition to nanomaterials having significant potential simply due to their reduced size, there exist fundamental phenomena that occur only at the nanoscale, many of which are either electronic or optical in nature.

Because certain nanomaterials are significantly smaller than the wavelengths of the visible spectrum of light, and because they are multi-component materials, new optical properties can arise from the *collective* response of the material upon exposure to light which are manifest neither at the macroscopic nor atomic scales. Indeed, gold (Au) and silver (Ag) materials with nanoscale dimensions strongly absorb light in the visible spectrum[12] and are actually responsible for the bright colors of stained glass windows found in many churches from the medieval period.

The phenomenon responsible for their optical activity is termed localized surface plasmon resonance (LSPR). LSPR has been explored in significant detail[13,14] and is currently an area of active research as these unique optical properties can be manipulated for a variety of applications, and the elucidation of these properties through both experiment and modeling will yield significant information about the fundamental electrodynamics at work in these

dimensions. As a simplified but illustrative example for explaining LSPR, a spheroidal Ag

nanoparticle can be envisioned as being comprised of two main parts: (1) a stationary core of

positively charged nuclei, and (2) a certain number of free conduction band electrons,

collectively referred to as a plasmon, which can be displaced relative to the electrons' original

positions by the electric field of an incident photon. With the assumption that, at any moment,

the entire particle experiences a homogeneous electric field since the diameter of the particle is

significantly smaller than the wavelength of light, a dipole charge separation will result. The

positively charged core of nuclei thus exerts a restoring force on the plasmon, similar to that of a

displaced spring, leading to a plasmonic oscillation about the positive core. Absorption then

occurs when the frequency of light is in resonance with the frequency of the plasmon oscillation.

The frequency at which this phenomenon occurs depends on the size, shape, composition, and

surrounding environment of the material. And, for relatively large particles significant scattering

of the light can occur as well. The summation of scattering and absorption effects yields an

overall extinction of various frequencies of light, which manifests itself in a surface plasmon

band (SPB) of easily-determinable width, shape, and λ_{max} by UV-vis spectroscopy in standard
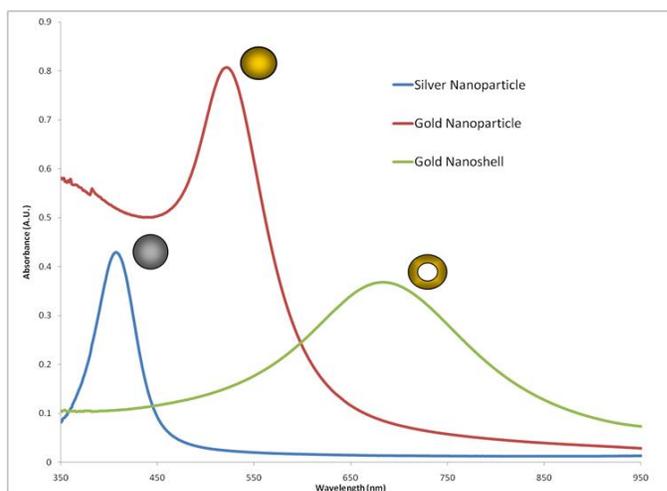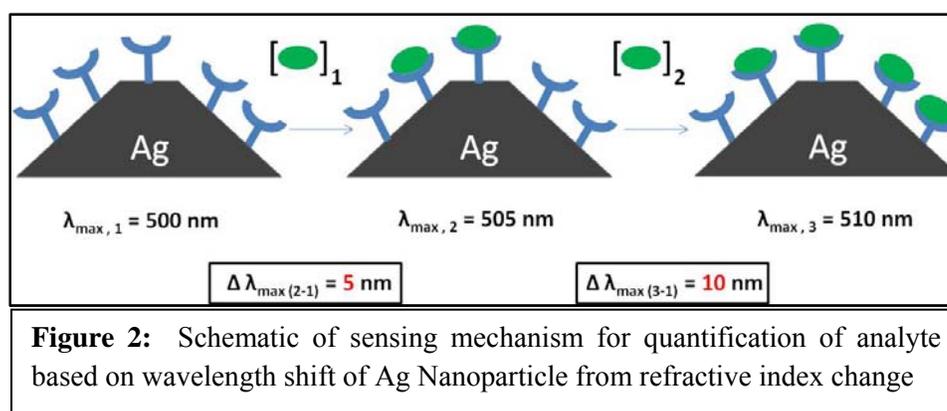
absorbance mode.

Figure 1: UV-vis absorbance spectrum depicting SPB's from various LSPR nanomaterials: Ag nanoparticles, Au nanoparticles, and Au nanoshells

Figure 1 shows the differences in peak shapes and peak locations of SPBs for Ag nanoparticles (λ_{max} = 420 nm), Au nanoparticles (λ_{max} = 520 nm) and hollow Au nanoshells (λ_{max} = 680 nm).

Sensing Applications

Due to this phenomenon, these optically active materials have potential in applications for the harvesting/amplifying/guiding of light. Also, as stated above, their optical properties are highly sensitive to their local environment, and thus can be easily affected and used as a detection signal upon the exposure of a given analyte for sensing technologies. With regard to sensing capabilities, there are two primary responses that can be induced by analyte exposure: (1) wavelength and/or intensity changes upon analyte binding at/near the particle's surface due to refractive index changes, and (2) wavelength, intensity, and/or peak width changes upon analyte-mediated changes in inter-particle distances due to increases or decreased particle-particle plasmon coupling.

Figure 2 schematically illustrates the wavelength shift caused by a change in refractive index for a potential sensing application. For example, in figure 2 a Ag nanoparticle, modified

Figure 2: Schematic of sensing mechanism for quantification of analyte based on wavelength shift of Ag Nanoparticle from refractive index change

with an arbitrary receptor, absorbs light with λ_{max} = 500 nm. Upon exposure to a certain concentration of analyte, binding of the ligand to the receptor occurs, increasing the refractive

index at certain areas on the surface, which subsequently causes the Ag-NPs λ_{max} to red-shift (i.e. shift to higher wavelengths of light). When a higher concentration of analyte is exposed to the system, more binding sites are occupied which increases the refractive index for more areas on the surface and causes a greater red-shift. Quantification of analyte is thus possible by correlating the particle's observed wavelength shift with the concentration of analyte. Other researchers[15,16], in attempts to detect analytes that are not able to change the refractive index to a discernible degree (e.g. small ions) or to create more specific techniques, have explored the use of analyte-mediated inter-particle distance changes as detection mechanisms. At small distances, the presence of one particle can have significant influences on neighboring particles, due to the coupling of two or more plasma. Plasmon coupling causes their λ_{max} to significantly shift to higher wavelengths, but the magnitude of the shift as well as the resulting peak shape of the SPB
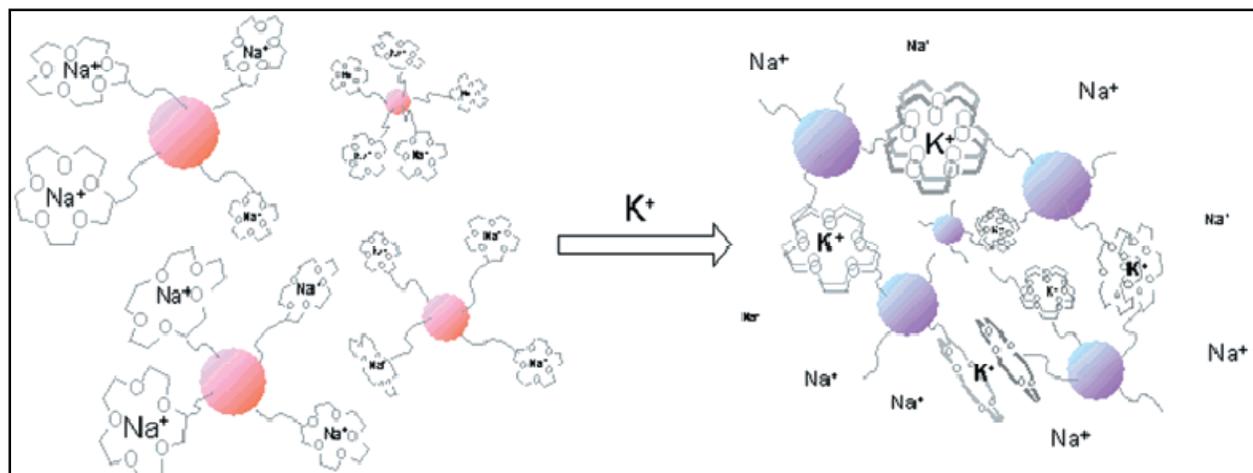
Figure 3: Schematic of sensing mechanism for quantification of analyte based on wavelength shift of Au nanoparticles upon analyte-mediated inter-particle distance changes (from ref. 15)

depends on the distance between particles. As an example, Chen et al.[6] detected potassium ions in aqueous solution by monitoring the optical response of coupled nanoparticles. The particles were functionalized with ionophoric crown ethers, which coordinate potassium ions in a 2:1 – crown-ether:potassium ratio. Thus, the coordination of potassium by two crown ethers on

adjacent nanoparticlse results in a visible change of the nanoparticles' solution color from red to purple.

Figure three shows isolated Au nanoparticles functionalized with Na+ coordinated crown-ethers (left), which, upon exposure to K+, coordinate in a 2:1 ratio from crown ethers of vicinal NPs (right), which allows the plasmons of the particles to couple resulting in a significant red-shift of the SPB. By monitoring the extent of aggregation spectroscopically, it is possible to determine the concentration of potassium in solution.

Many of these sensing systems are solution-based. Incorporating these materials within ordered arrays or thin film systems that are easy to prepare, highly stable in various environments (organic, aqueous, ambient air), and that do not lose their sensing abilities when confined to a more restrictive geometry holds significant promise for developing cheap, disposable, and versatile sensors. [17]

Introduction

Ordered Arrays

There are, in fact, a variety of methods for specifically guiding the assembly of nanomaterials via different linking mechanisms.[18] Mirkin et al.[19] have extensively explored the use of complementary thiolated DNA strands adsorbed to nanoparticles to create larger aggregated structures; and, by selectively choosing the length of the DNA strand, they have been able to systematically order the nanoparticles at arbitrary distances. Others have utilized polydentate ligands to arrange nanoparticles,[20] which involves coupling two particles by a dithiol where one thiol is chemisorbed to one particle and the second thiol to the other particle. And yet others have connected particles by covalently coupling the terminal functional groups of adsorbed ligands on

adjacent particles (e.g. primary amines with carboxylic acids).[20] Electrostatic interactions from oppositely charged polymers (polyelectrolytes) with charged nanomaterials is also an effective vehicle for guided assembly.[17]

<u>Polyelectrolyte Film Systems</u>

Much of the work discussed in the present thesis has been an attempt to rationally design, assemble, and characterize multilayered films systems comprised of nanomaterials and polyelectrolytes for sensing applications that could not be accomplished by any of the two individually. Although these two systems (i.e. nanoparticles and polyelectrolyte films) have been explored extensively as individual systems, the efficient combination of the two is a relatively unexplored field. One hypothesized scheme that could be employed for a sensing system involves functionalizing the NPs within the film with analyte-specific ligands, exposing the films to the analyte, and detecting a measurable optical response from the nanoparticles via standard Uv-vis absorbance measurements. As stated previously, this optical response could arise from either refractive index changes, which is indeed feasible due to the semi-porous nature of the films, or from inter-particle distance changes, which is also possible due to the flexible nature of the films.

The exploration in multilayered-polyelectrolyte systems for constructing a thin film for sensing with optically active nanomaterials was motivated by several potentially advantageous characteristics: (1) depending on the composition of the polymers, the porosity of the film can be manipulated such that an analyte (small in comparison to the nanoparticles) can freely and rapidly diffuse in and out of the film; whereas the nanoparticles cannot easily escape the film due to their large size and number specific interactions; (2) analyte-mediated inter-particle distance

changes are feasible given that the film geometry remains flexible for small diffusion or movement; (3) multiplexed sensing could be achieved by differentially isolating various analyte-specific nanomaterials in different regions of the film; (4) stability enhancements of the nanomaterials in films over solution are envisioned because the polyelectrolytes can serve as physical barriers for irreversible aggregation events that may occur more easily in solution upon drying; (5) the distance between nanomaterials can be controlled during the assembly process for optimizing a given application that requires a specific and well-defined interparticle distance; (6) film growth is facile and rapid (i.e in comparison to other film growth methods such as the Langmuir-Blodgett film system) due to the well-developed layer-by-layer(lbl) dip-cycle method described below.

These LBL polyelectrolyte films have been extensively explored by Decher et al. [21] Leopold et al. [17] showed their use as a rapid method for incorporating single layers of poly-l-lysine between Au nanoparticles. This general technique has subsequently been extended to more complex systems where *multiple* layers of oppositely charged polyelectrolytes exist between the nanomaterials layers;[22] a general schematic for the design is shown in figure 4.
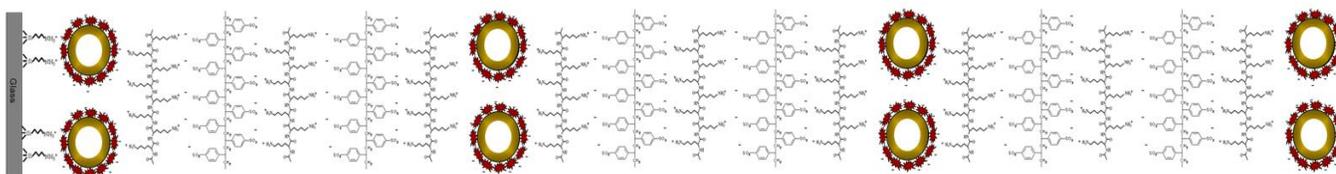
Figure 4: General design of a 5L multilayer-polymer multilayer-nanoshell film attached to a glass slide. 5L refers to the 5 layers of polymer (PLL and PSS) between the nanoshell layers. The glass substrate is modified with an amine terminated silane.

The process involves the silanization of a glass slide with amine-terminated molecules that serve as the positively charged deposition surface, to which an initial layer of negatively charged NMs is deposited by exposure to the NM solution. The glass slide with the first layer of

negatively charged NM is then exposed to a solution of positively charged polymer, poly-l-lysine, which forms a stable layer due to multiple electrostatic interactions. A series of exposures to oppositely charged polymer solutions (i.e. polystyrene sulfonate (PSS) = - , poly-l-lysine (PLL) = +) can be performed to grow the polyelectrolyte films to a desired layer number (x L – where x is the number of layers); the slide is exposed again to the NM solution, which forms a second layer of NM on the slide. For clarification purposes, it should be noted that figure 4 illustrates a 5L multilayered-polymer multilayered-NM.

The entire dip cycle process can be repeated again to grow the films to a desired thickness/height. In fact, improving these systems by changing the number of polymer layers between NM layers from 1 layer (1L), to 3 layers (3L) to 5 layers (5L) and measuring their optical responses is of interest for the present work. Additionally, much of the work has been dedicated to exploring the growth dynamics, stabilities, and optical properties of these multilayer-polymer multilayer-NM systems for eventual sensing applications. A proposal for better understanding the effects of refractive index and of inter-particle coupling follows the results and discussion.

Experimental

Chemicals:

Poly-L-lysine (PL, MW = >30,000), poly(4-styrene sulfonate) (PSS, MW = 75,000) were purchased from Sigma/Aldrich and used as received. All polymer linkers were dissolved in chilled sodium phosphate buffer (8.8 mM, pH 8.5) to yield 0.5 mM solution concentrations. All reagents and modifying alkanethiols were purchased commercially and used as received with the

exception of the 15-crown-5 terminated alkanethiols which were synthesized and prepared as previously reported.[15] Ultrapure (UP) water (18 MΩ) was used for all experiments unless noted otherwise.

Instrumentation: Optical measurements were obtained with UV–Vis spectroscopy in standard absorbance mode by an Agilent 8453 Photo Diode spectrometer. Transmission electron microscopy (TEM) imaging was performed at 80 kV operating voltage with samples of drop-casted NP/NS solutions on 400 mesh copper grids coated with Formvar and carbon (Electron Microscopy Sciences).

Au nanoparticle synthesis and modification:

Gold nanoparticles (d = ~ 10 nm) capped with citrate were synthesized by the rapid addition of a 38.8mM solution of sodium citrate to a boiling aqueous solution of 1 mM $HAuCl_4$ which underwent a color change from light yellow to clear to dark ruby red. [25] The solution was cooled to room temperature after a 10 minute reflux. The Au Nps were then further functionalized by adding thioctic acid in a TA:Au molar ratio of 1:1 after adjusting the pH of the solution to pH = ~11 with 0.5 M NaOH. After stirring overnight in the dark, the TAS-NP solution was cleaned by centrifugation (15,900g, 25min, 10^0 C), and re-suspended in water.

Hollow Au nanoshell synthesis and modification:

Hollow gold nanoshells (NSs) (d= ~ 22 nm) were synthesized according to a procedure developed by Xia and Sun in which an aqueous solution of $HAuCl_4$ reacts with silver NPs, which serve as sacrificial templates [26] (see Fig. 1). For a typical Ag NP synthesis [27], 0.400 g $AgNO_3$ in 15 mL ethylene glycol was added to a solution of 10 g polyvinylpyrrolidone (PVP) in 50 mL

ethylene glycol upon the complete dissolution of both solids. The reaction mixture was then refluxed for ~12 h in an oil bath at 120° C with stirring. The final PVP-stabilized Ag nanoparticles were redissolved in 100 mL water and stored in the dark after washing with 200 mL acetone and centrifugation (10,000 rpm, 20 min, 10^0 C). To synthesize the Au nanoshells, a dilute solution of Ag nanoparticles was refluxed for 10 min, at which point a 1 mM HAuCl4 aqueous solution was slowly added dropwise. With the addition of gold salt, the reaction progresses with the simultaneous reduction (deposition) of gold salt at the expense of the oxidation (dissolution) of the solid Ag templates and can be monitored by UV/Vis spectroscopy. Upon the disappearance of the surface plasmon band (SPB) of the Ag nanoparticles (λmax = ~ 420 nm) and the development of the SPB of the Au nanoshells (λmax = ~ 680 nm), the addition of gold salt was terminated, and the mixture was refluxed for a final 20 min. Modification of Au nanoshells was accomplished by mixing a 5 mM mercaptoundecanoic acid (MUA) ethanol solution with the "as prepared" nanoshells in a 1:500 molar ratio for ~5 h. The pH was adjusted to slightly basic conditions (pH = ~8) with 0.5 M NaOH to ensure the retention of electrostatic repulsion of NSs from the terminal carboxylic acids during centrifugation at 10,000 rpm for 30 min. The resulting pellet was then reconstituted in water for eventual incorporation into various film assemblies.

Film Growth

Nanomaterial films were all grown using precut, Piranha-cleaned glass slides. [*Warning! Piranha solution (2:1 conc. H2SO4 to H2O2) reacts violently with organic materials, handle with extreme caution!*] Glass slides were silanized with 3-(aminopropyl)trimethyloxy silane (3-APTMS). Films were grown using the "dip cycle" method, where growth materials are adsorbed

onto the film by dipping the slides in alternating aqueous solutions. [23,24] The glass slides were dipped in either TAS-NP or PVP-NS solution for 1 h followed by 30 min dips in the appropriate polymer solutions, and then again for 1 h in NPs or NSs (dip cycle). The films were rinsed with UP water in between dip solutions, and stored in UP water. PLL and PSS dip solutions were refrigerated during both film growth and storage. Film growth was monitored by UV–Vis spectroscopy every two completed dip cycles by placing the glass slide in an UP water-filled cuvette. Dip cycles were repeated for eight layers, or until the multilayered film was of the desired absorbance, around 0.1 AU measured at 400 nm (NP) or 600 nm (NS) - wavelength positions, which are removed from the surface plasmon band (SPB) so as to avoid recording any optical changes affecting the size, shape or position of the SPB as a change in film absorbance/thickness. [28] In general, the initial monolayer or submonolayer of NPs on the modified glass substrate is pinkish-red in appearance, matching that of the NP dipping solution, and displays a spectrum featuring a SPB at 520 nm.

Results and Discussion

Various types of multilayered-polymer multilayered-NM films were grown by alternately exposing the glass slides to aqueous solutions of poly-l-lysine (PLL), polystyrene-sulfonate (PSS), and NMs as described above.

1. Multilayer-polymer multilayer-nanoparticle films

A. Film Growth

Figure 5 (left) shows the successful growth of 1L (PL), 3L (PL/PSS/PL), and 5L (PL/PSS/PL/PSS/PLL) multilayer-polymer multilayer-nanoparticle films. With alternating exposures to polymer and nanoparticle solutions (Note: each exposure to nanoparticle solution constitutes one dip cycle), the absorbance of the film at 400 nm increases linearly with dip cycle.
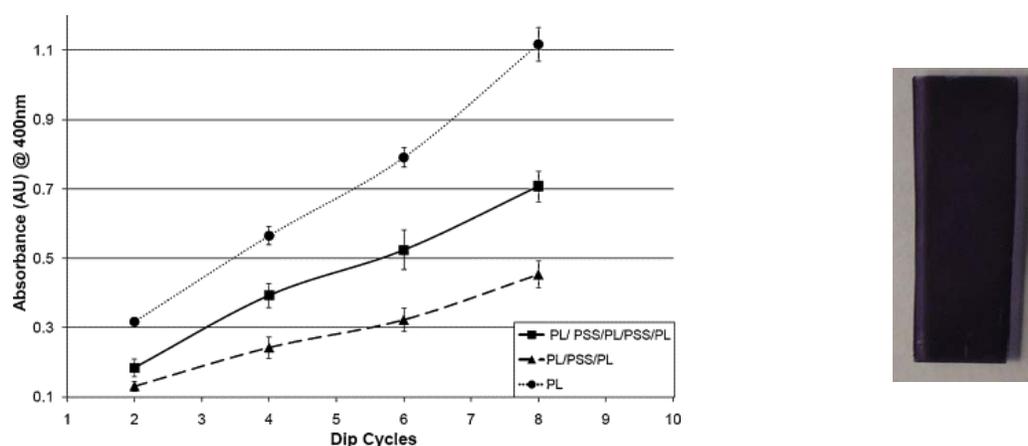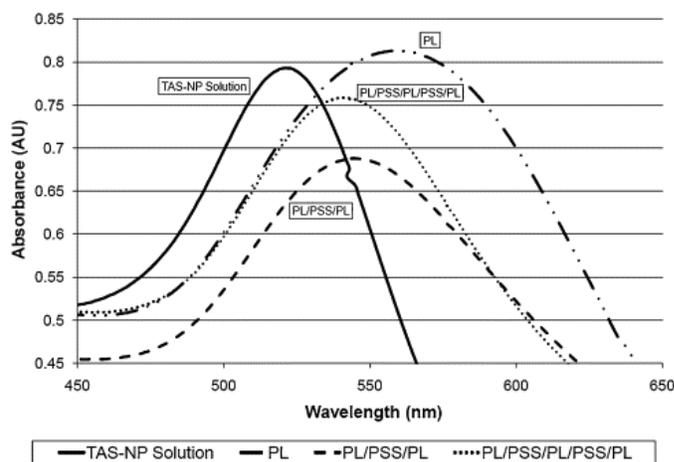

Figure 5: (left) Film growth comparisons of 1L(PLL) , 3L (PLL/PSS/PLL), and 5L (PLL/PSS/PLL/PSS/PLL) multilayer-polymer multilayer-nanoparticle films. (right) Actual image of 5L multilayer-polymer multilayer-nanoparticle film system on a glass slide. [From ref. 22]

This indicates film growth because the steady increase in absorbance suggests that additional layers of NPs are being deposited.   Figure 5(right) is an actual image of a 5L multilayered-polymer multilayered-NP film, indicating that the film is evenly distributed on the glass slide, and that the film itself can easily be seen with the naked eye.

The differences in the actual dynamics of the growth are evident from the slopes of the lines with 1L growing faster and to a higher overall absorbance than 5L, and 5L similarly than 3L; the current paper is not concerned with these differences in regards to rate of growth, but detailed discussions for the interested reader can be found in ref (22).

B. Optical Properties

Since Au NPs are optically responsive to their local environment, a comparison of the

SPBs for nanoparticles in solution with NPs in various film geometries is of interest. Figure 6

displays the SPB of thioctic-acid stabilized gold nanoparticles (d = 10 nm) in aqueous solution

with a $\lambda_{max} = \sim 520$ nm. In solution the nanoparticles' plasmons do not couple because

Figure 6: UV–Vis spectra comparing SPBs of 1L (PLL), 3L (PLL/PSS/PLL) and 5L (PLL/PSS/PLL/PSS/PLL) multilayer-polymer multilayer-nanoparticle films compared TAS-NP in solution [From ref. 22]

electrostatic repulsion from the deprotonated carboxylic acids at the NP surface prevents the NPs

from approaching distances necessary for coupling to occur. When a multilayered film is

constructed however, the presence of the positively charged amines on the poly-l-lysine reduces,

to some extent, the inter-particle electrostatic repulsion. This confines the NPs to significantly

decreased distances such that the plasmons of the particles are able to couple, resulting in a

collective SPB for the film that is significantly red-shifted and broadened with $\lambda_{max} = \sim 570$nm in

comparison to NPs in solution. The observed broadening could arise from plasmon coupling of

particles at non-uniform distances within the film. For example, the distance between particles

near the glass substrate may be less than that of NPs nearer the solution interface since it has

been shown that the packing density of polymer layers in multilayer polyelectrolyte films

decreases with increasing distances from the substrate, and is also affected by the total film thickness.[29] Therefore a broadened SPB at 570 nm could be the summation of distinctive plasmon bands located at wavelengths less than and greater than 570 nm.

Indeed this inter-particle distance dependence on the location of the λ_{max} of the film is evident from the λ_{max} s of the three (PLL/PSS/PLL) and five (PLL/PSS/PLL/PSS/PLL) linking bridge system. (figure 6) As the number of polymer layers increases between particle layers (i.e. in going from 1L to 3L to 5L), the distance between particles increases and the magnitude of the response from coupling decreases. This decreased coupling results in film λ_{max} s that are to the blue of the single linking bridge system with 3L - λ_{max} = ~545 nm and 5L - λ_{max} = ~540 nm. A qualitative decrease in peak broadening for these systems in comparison to the 1L is also apparent. Although extending the system to a greater numbers of polymer layers might further increase the distance between NP layers, it is likely that no film system would be able to achieve a film λ_{max} similar to a λ_{max} of NPs in solution due to lateral NP coupling that can occur within a given NP layer. However, the position of the SPB for these film systems is not due entirely to particle-particle plasmon coupling since red-shifts are also caused by the increase in refractive index at the particle's surface upon polymer-layer formation. For this reason, it is not possible to accurately quantify the relationship between the number of polymer layers between particles with their optical responses.

**2. Multilayer-polymer multilayered-nanoshell films**

A. Film Growth

As it was determined that the 5L multilayered-polymer multilayered-NP film system was effective for creating films that were solution- as well as air-stable[22] the design was extended to the construction of films comprised of hollow gold nanoshells (NSs). These materials have been shown to exhibit significantly increased optical sensitivities to changes in their local environment compared to solid gold nanoparticles of similar sizes; thus, it was hypothesized that the increased sensitivity over the solid particles would be manifest within the films as well, and potentially lead to applications with enhanced responses over the NP films.
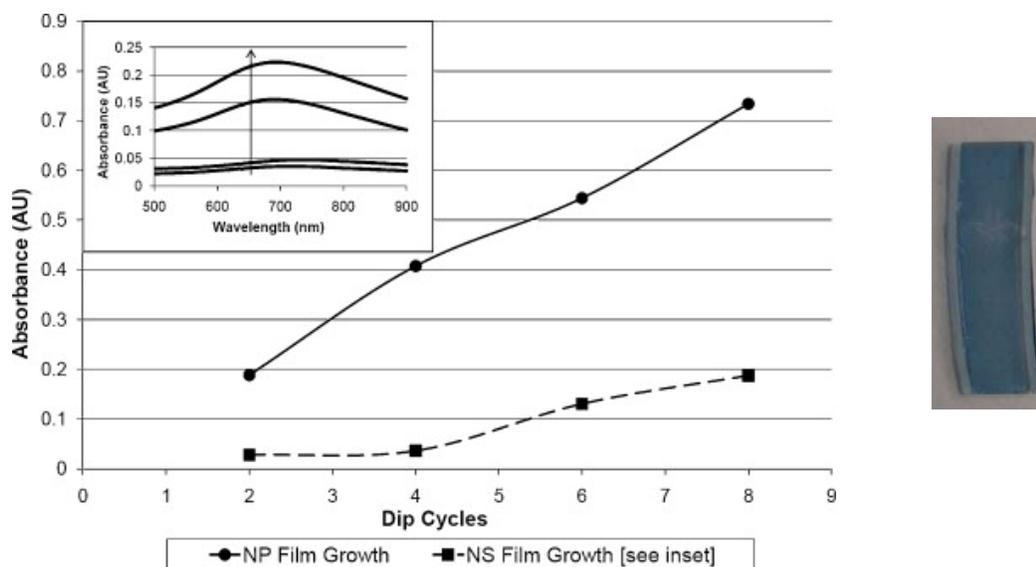
Figure 7: (left) Film growth comparisons of 5L (PLL/PSS/PLL/PSS/PLL) multilayer-polymer multilayer-nanoshell film to that of a multilayer-polymer multilayer-nanoparticle film. (right) Actual image of 5L multilayer-polymer multilayer-nanoshell film system on a glass slide. [From ref. 22]

For the NSs, successful film growth was also achieved with solution- and air-stability observed as well. One can also see the actual image of the NS film in figure 7 shows the growth of a 5L (PLL/PSS/PLL/PSS/PLL) multilayer-polymer multilayer-NS film upon alternating

exposure to polymer and NS aqueous solutions. With the same number of dip cycles, the growth

rate (indicated by slope) and overall absorbance maximum of the NS film appear lower than that

of the analogous NP film for reasons which are presently unknown; however, it is hypothesized

that this difference in film growth might result from the difference in size of the NSs (d = ~

35nm) and NPs (d = ~ 10 nm). Further discussion is continued in ref (22).
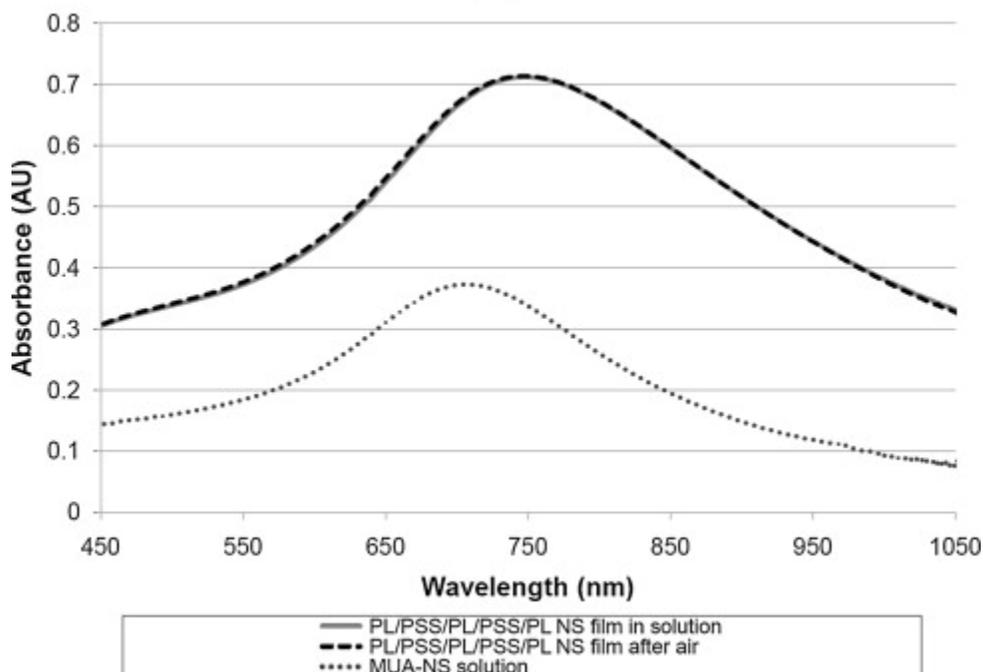
Figure 8: UV–Vis spectra showing SPB of (a) NS film in solution, (b) NS film in solution after exposure to air, and (c) a solution of NSs.

B. Optical Properties

Similarly for the NPs it is important to compare the optical response of NSs in solution

with those in restricted film geometries. Figure 8 shows the SPB of the MUA-stabilized hollow

gold nanoshells (NSs) in solution with λ_{max} = ~700 nm compared to the SPB with λ_{max} = ~ 750

nm from a 5L multilayer-polymer multilayer-NS film (Note: The SPB of the NSs in solution is

inherently red-shifted (λ_{max} = ~700 nm) as compared to the solid gold nanoparticles' SPB, and so

it should be noted that this is not a result of aggregation or plasmon coupling.) Similar to the NP system, upon incorporating the NSs into a film, a red shift of the SPB is observed, as well as a change in its peak shape at ~ 900 nm.

In addition, interesting trends were observed during the growth of the multilayer NS films that were either nonexistent for the particle films or, more likely, present but with a response of much smaller magnitude.   Indeed, significant shifts occurred upon the deposition of *each* polymer layer, indicating that the deposited NSs were extremely sensitive to refractive index changes from a *single* layer of polymer formation.

1. Optical Sensitivity Comparisons: NPs vs. NSs

A. Solution Comparisons

One of the purposes of this work is to directly compare the optical sensitivities of gold NSs to gold NPs. To accurately compare their sensitivities, experiments were first performed in solution so that inter-particle plasmon coupling effects would not confound the results – a process which inherently must occur within film geometries. It is well known that straight-chain alkane thiols form well ordered self-assembled monolayers (SAMs) on noble metal surfaces, and they are commercially available in a variety of lengths; therefore, their self assembling formation on the NP/NS surface is a facile and highly controllable way to probe the short range distance-dependence of refractive index changes on SPB shifts. Furthermore, shifts induced by SAM formation are strictly due to refractive index changes and not inter-particle plasmon coupling.

Thiols of various chain lengths (n = number of methylene units in hydrocarbon backbone of ligand) and of various terminal functional groups (i.e. carboxyl, methyl, hydroxyl) were added to solutions of either NPs or NSs. The change in λ_{max} upon SAM formation was plotted as a function of chainlength (n) in figure 9; the results of which experiments yielded several
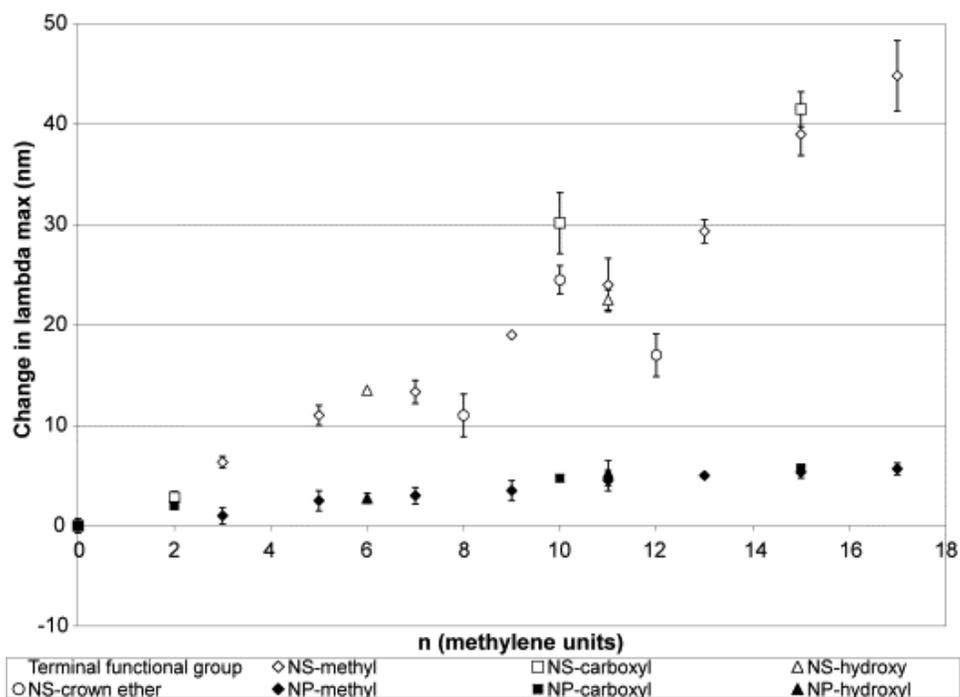

Figure 9: Changes in the λ_{max} of the SPB for solutions of NPs (solid symbols) and NSs (open symbols) as a function of the alkanethiol chainlength (i.e., methylene units, *n*) and terminal functional groups (-CH$_3$, -OH, -COOH, 15-crown-5). Note: The error bars refer to the standard deviation of an average based on measurements of three replicates. Some points have error bars that are smaller than the marker associated with that average

interesting trends. First, the $\Delta\lambda_{max}$ for both materials increased linearly with an increase in the length of the hydrocarbon backbone, which was not unexpected since the SAM should increase the refractive index around the particle. Second, it is clear that for a given thiol chain length, n, the magnitude of the response from the NS is significantly greater than that from the NP. For example, the C18 methyl-terminated thiol induced a $\Delta\lambda_{max}$ of ~ 6 nm for the NP solution, whereas a ~ 45 nm red-shift was noted for the NS solution. Both of these trends reiterate similar sensitivity results shown by Xia and co-workers with alkanethiol derivatives of NSs. Another

point of interest was also the *insensitivity* of both systems to the different terminal functional groups. With results falling approximately on the same slope for each set of terminal-functional group alkanethiol, the shifts in the SPB seem to depend only on the chainlength of the adsorbed ligand.

B. Film Comparisons

Since the NSs exhibit significantly enhanced optical sensitivities in solution compared to solid NPs in response to the same binding events, inquiry was made as to whether this greater sensitivity would be diminished when incorporated into these film systems. To test this, two 5L multilayered-polymer multilayered-NM films of both NPs and NSs were exposed to C4 and C14 alkanethiol in solution and their optical responses were recorded. Figure 10 shows the SPB
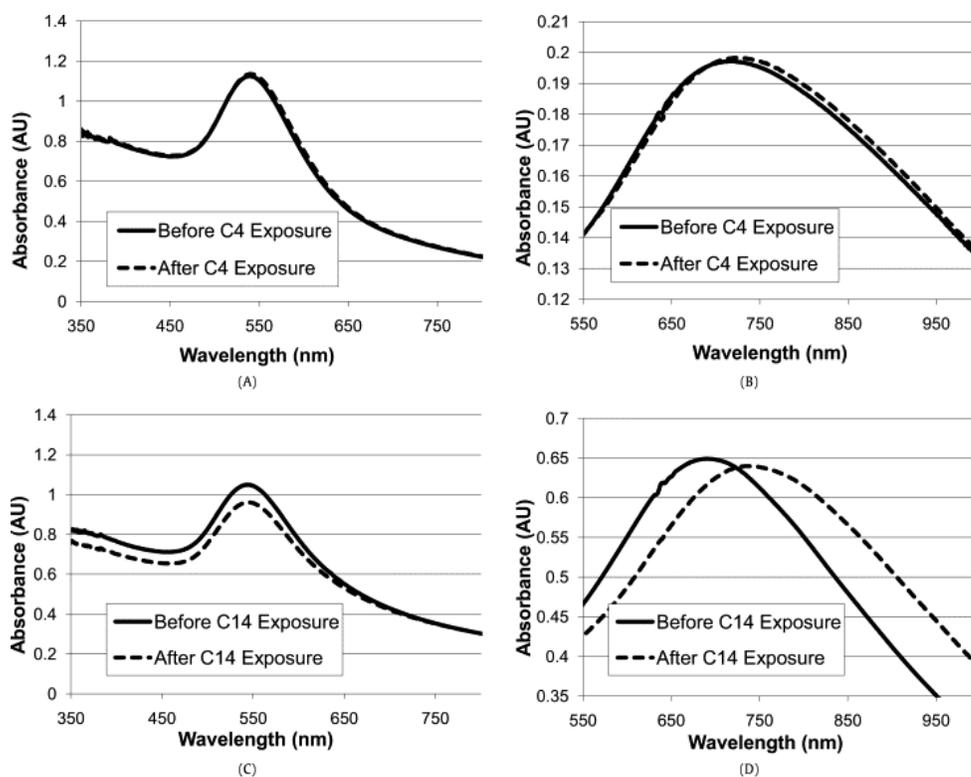
Figure 10: UV–Vis spectra showing SPB of NP film (A and C) and NS films (B and D) before and after exposure to 5 mM butanethiol (top) and tetradecanethiol (bottom) ethanol solutions for 30 min followed by copious rinsing before being reimmersed in water for absorbance measurements.

before exposure to the thiol in solution (solid), and after an hour exposure (dotted) to the appropriate thiol in solution. For both NP films (a and c) a minimal change in the SPB was observed after exposures to C4 as well as C14. The NS film (B) exposed to C4 exhibited a noticeable but small response, whereas the C14 exposure induced a significant red-shift of ~ 50 nm. From these preliminary results, it is clear that the NSs do, in fact, retain their enhanced sensitivities for both C4 and C14 even when confined to a film geometry, which suggests their possible use within portable, stable film sensing system.

4. Summary: Film SPB shifts from refractive index changes and plasmon coupling

It is apparent from the discussion above that a multilayer-polymer multilayer-NM film has a collective SPB whose λ_{max}, wavelength shifts, and peak broadening are influenced by a multitude of factors including inter-particle plasmon coupling and changes in the refractive index at the surface of the particle. This combination of influences makes the accurate representation and modeling of these systems difficult. Thus, in order to quantitatively understand the underlying processes, subsequently manipulate, and ultimately optimize these effects for a given sensing application, the response of a film's SPB needs to be comprehensively analyzed by differentiating between refractive index changes and inter-particle coupling effects.   The following proposal is an attempt to systematically elucidate the various influences on optical responses from different "microenviroments" within the film, and determine how these "microenvironments" vary throughout the film.

Thesis Proposal

Introduction

These multilayer-polymer multilayer-NM film systems exist as a single cohesive material whose macroscopic properties arise from the summation/combination of all the different "microenvironments" or "microdomains" within the film. When certain macroscopic measurements of a system are obtained (e.g. density of material in the film, dielectric constant of the film, or more specifically the SPB for these film systems), it can easily be assumed by various arguments that these properties are not uniform over the entirety of the film system but rather are averages from a wide range of values. For example, an absorbance measurement of a film with a broad SPB and $\lambda_{max} = 700$ nm might be an average of particles absorbing in the range of $680 - 720$ nm; however, the SPB could also result from a set of particles with $\lambda_{max} = 700$ nm whose broadening is brought about by a refractive index or structural change that occurs upon film incorporation. These two examples yield the same macroscopic response but result from entirely different phenomena occurring within the microenvironents. Therefore, for the optimization of any potential sensing system, it is obviously necessary that the types of microenvironments as well as the weight of their respective responses to the overall response of the system be explored in detail.

Microenvironments in nanoshell films

Specifically for these multilayer-polymer multilayered-NS films, there are three major interacting components: (1) the glass substrate, (2) the actual film itself, which can further be subdivided into the (a) the various polymer layers and (b) the nanoparticles, and (3) the film/air or liquid interface (Figure 11). In order to understand the distribution and inhomogeneity of the
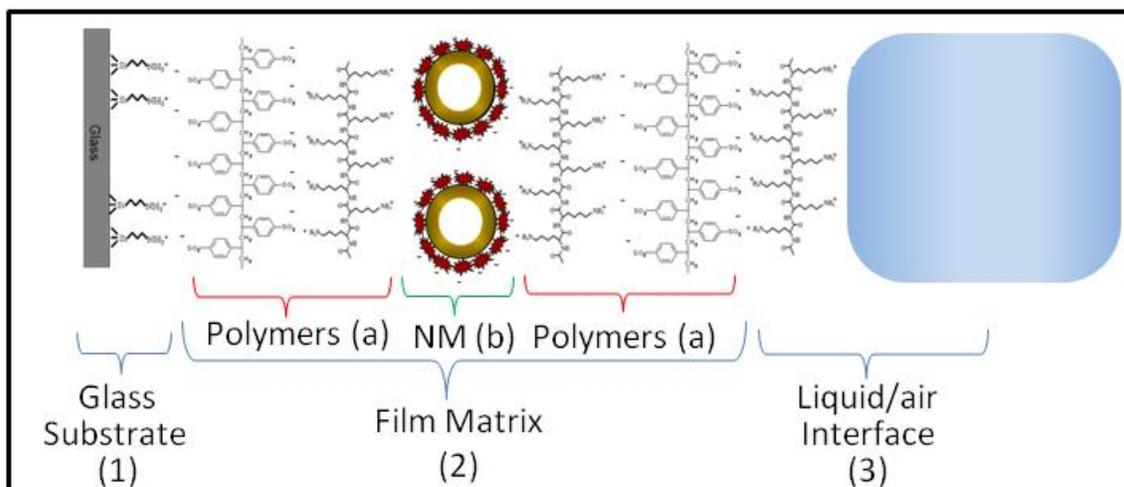
Figure 11: General design of multilayer-polymer nanoshell film, highlighting the three main components

5L multilayer-polymer multilayer-NM film systems, the contributions of the optical responses from various populations within the film system need to be individually isolated and appropriately characterized. It is likely that these NMs within the multilayered film are distributed somewhat randomly throughout and constitute a wide spectrum of microenvironments; however, for simplification it is necessary to condense these NSs into three general populations based on the three main aforementioned components: (A) NSs directly adsorbed to or near the glass substrate, (B) NSs within the polymer film matrix, and (C) NSs near the film/air or liquid interface.

These populations have been differentiated as such for several reasons. As mentioned previously, the packing density of polymers depends on the distance from the substrate along with the total film thickness where the density tends to be greatest nearer the substrate, and as the overall thickness of the film increases. A high polymer packing density should have two effects: the refractive index should be higher, and the interparticle distance should decrease, both of which, although difficult to separate, cause red-shifts.

Also, the refractive index varies throughout the film. Populations A and C should have significantly different dielectric environments due to the presence of the glass substrate and the

interface respectively. Population B will similarly be affected by both of these components as well, but the exact distance dependence of these influences is not known quantitatively. The dielectric constant of the neighboring nanoparticles will also affect the response of a given population of NMs but the density of the particles needs to be known.

Research Plan

For the multilayer-polymer, multilayer-nanoparticle films described in the results section above, multiple exposures of the film to the nanoparticle solution are employed to alternately deposit polymers and nanoparticles; thus, the film's λ_{max} is a sum of the optical contributions from each different nanoparticle layer. The increased optical sensitivity of the Au-NS to its local environment therefore makes it an ideal candidate for investigating the various microenvironments in the film such that even a single polymer layer deposition should elicit a discernible response. In order to determine the contributions from individual microenvironments or layers, a series of multilayer-polymer/***monolayer***-NS films (in contrast to the multilayer-polymer/multilayer-NS films)

Substrate Effects

To determine the effect of the substrate and its distance dependence, several films will be grown with a constant overall number of polymer layers, L = 35; the only difference between the films will be the location of the monolayer of NSs. Figure 12 displays 3 representative types of films for this experiment.
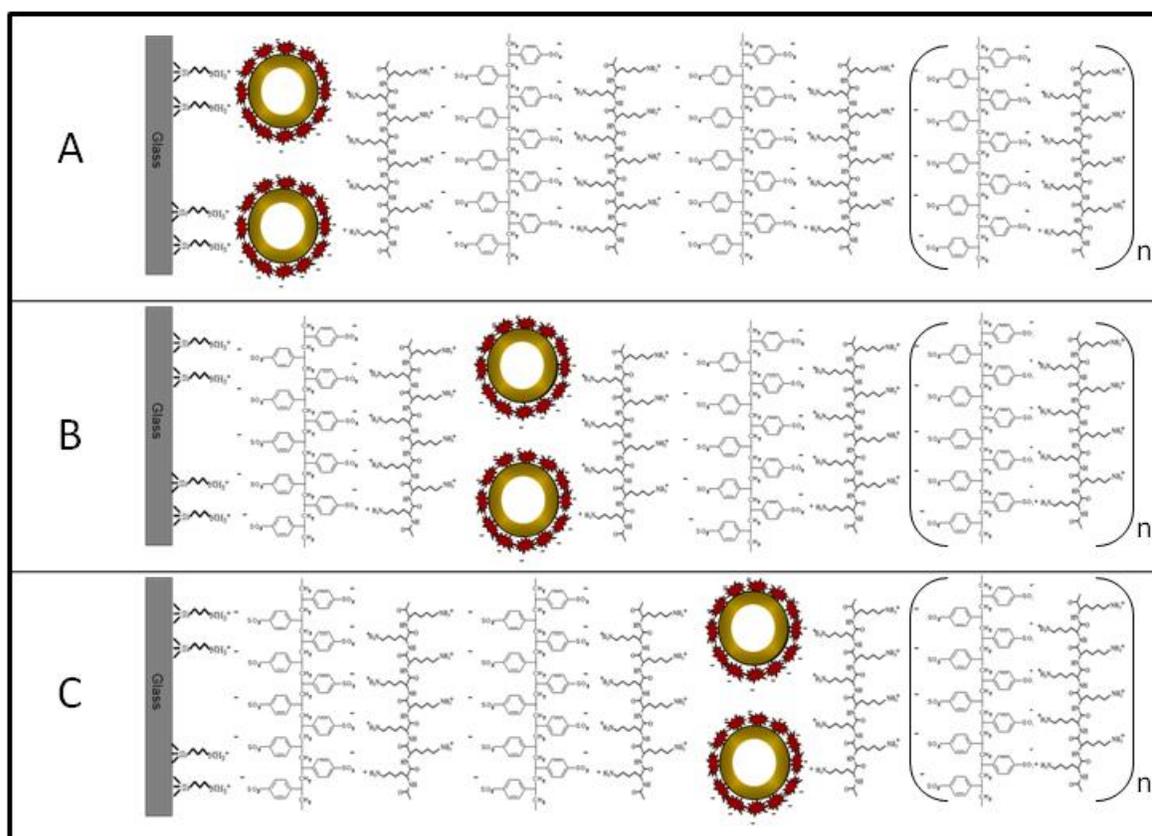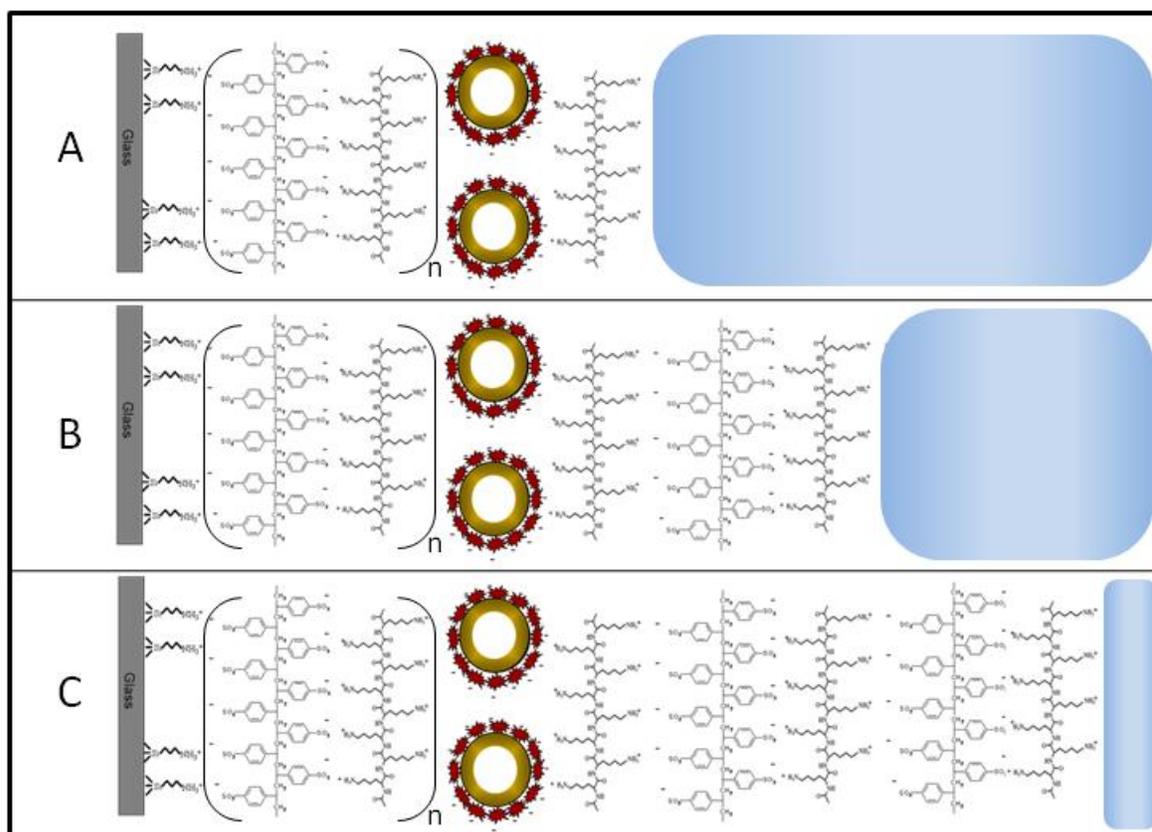
Figure 12: Substrate effects on optical response of a nanoshell. Three multilayer-polymer monolayer-NS film designs with 0(A) , 2 (B), and 4(C) polymer layers between substrate and NS monolayer with brackets denoting the continuation of film growth with n = 15.

For film A, NSs will be directly adsorbed to the substrate followed by 35 alternating depositions of PLL and PSS. For film B, two layers of polymer (PSS and PLL) will be deposited to the substrate followed by exposure to NS solution, and then the remaining 33 polymer layers. In a similar fashion, the rest of the films within the series will contain two additional polymer layers between the glass and the NSs. This process systematically controls the distance between the NSs and the substrate without changing the overall thickness of the film, which will lend insight into the influence of the glass slide on the optical response of the NSs and its dependence on distance.

Interface Effects

As the above procedure will determine the effect and distance dependence of the glass substrate, the same effect of the interface can be explored by systematically changing the number of polymers between the NSs and the interface.
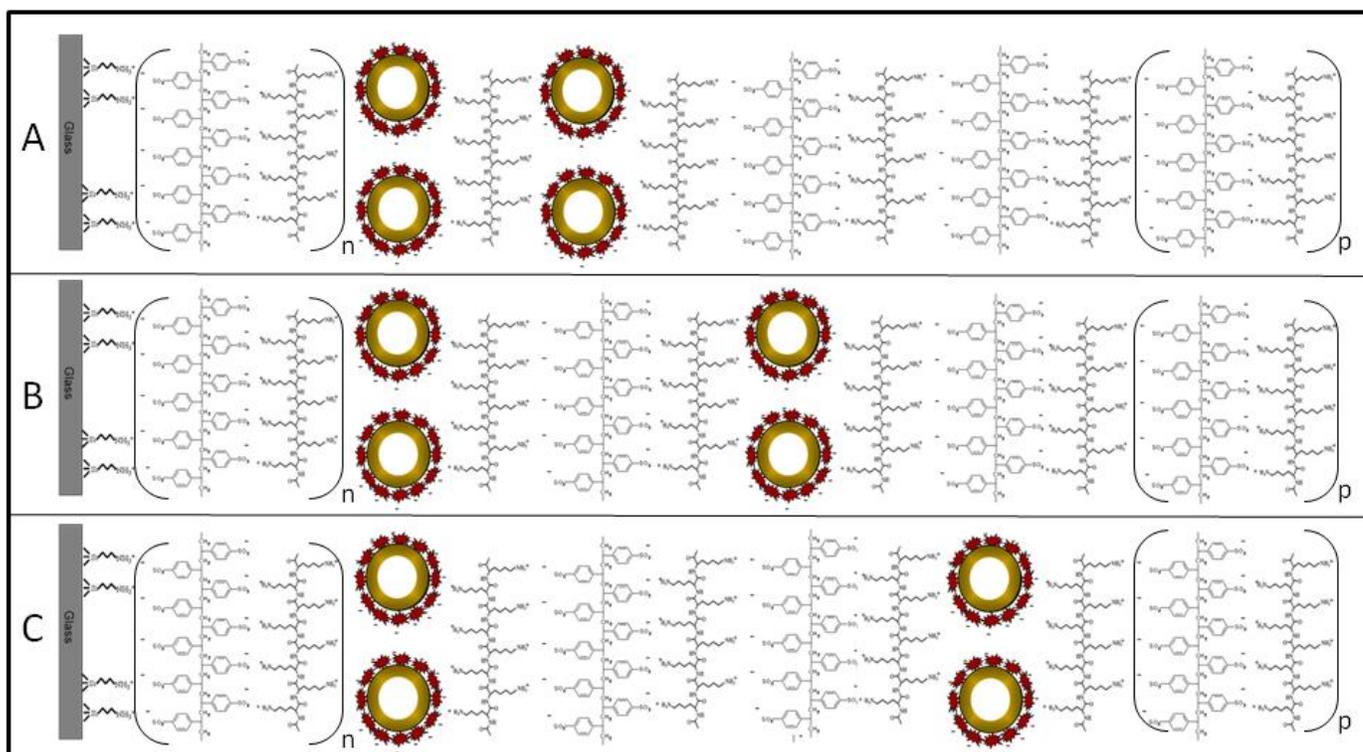

Figure 13: Interface effects on optical response of a nanoshell. Three mulilayer-polymer monolayer-NS film designs with 1(A) , 3(B), and 5(C) polymer layers between NS monolayer and interface, with a constant distance from substrate (n = 15). Shaded figure denotes the film-solution/air interface

For these experiments, the distance between the glass substrate and the NSs will be constant (n=15) but the number of polymer layers between the NS monolayer and the interface will be changed. For film A, the film will be exposed only once to the solution of polymer after monolayer-NS formation. For film B, three layers of polymer will be deposited to the film

following the exposure to NS solution. In a similar fashion, the rest of the films within the series

will contain two additional polymer layers between the NSs and the interface. This process

systematically controls the distance between the NSs and the interface without changing the

distance from the substrate, which will lend insight into the influence of the interface on the

optical response of the NSs and its dependence on distance.

Interparticle Coupling Effects

Once the effects from the substrate, polymer, and interface on different NS populations

have been elucidated fully, it will be necessary to explore the inter-particle interactions to further

understand the dynamics of the film. Depending on the type of film (1L, 3 L, 5 L) differing

amounts of polymer layers are interspersed between the nanoparticles. Multiple layers of

nanoshells could grant an additional desired complexity to the system, with potential for

multiplexed systems by the use of differently functionalized NS layers. To explore the distance

dependent coupling of two layers of NSs, various multilayered-polymer/bilayered-NS films will

be constructed with different distances between the NS layers. Figure   depicts the proposed

schematic for these experiments.

Figure 14: Interparticle coupling effects on optical response of nanoshell. Three mulilayer-polymer bilayer-NS film designs with 1(A) , 3(B), and 5(C) polymer layers between NS bilayers, with a constant distance from substrate (n = 15) and constant distance from interface (p = 15)

A legitimate concern that has not been neglected by this proposal is whether the NSs actually exist as distinctly isolated layers or, contrariwise, if they permeate and randomly distribute themselves throughout the film over time. It is presently hypothesized that the nature of the film matrix will be relatively resistant to significant translocation of the NSs due to the large relative size of the NSs, and the high molecular weight and high packing density of the polymers; however, several techniques can be employed to test this assertion. Rapid diffusion of the NSs homogeneously throughout the film would result in identical λ_{max}s for the films described above for the variously positioned monolayers – evidence which is not currently supported by preliminary experiments. Slow diffusion (i.e. over the course of hours, or days)

could be easily monitored by UV-Vis measurement taken over time, or could even be actively initiated through annealing. Additional evidence will be provided through a relatively non-conventional TEM imaging method. If, on the other hand, it is discovered that the NSs are in fact able to significantly diffuse throughout the film, it will be possible to explore ways to restrict this diffusion, either by optimizing conditions (e.g. ionic strength, pH, low temperature, etc.), or by effectively tethering the NSs together via covalent linkages.

Conclusion

The growth of various multilayer-polymer multilayer-nanoparticle and nanoshell films was accomplished. The nanoshells exhibited significantly enhanced optical responses over gold nanoparticles to the same binding events in solution and films. The nanoshells are proposed to be used as optical reporters of the various microenvironments in these film systems. The elucidation of the subtle differences of the microenvironments in the films will hopefully improve the understanding of the film systems as well as the sensing capabilities of these NSs.

References

1. Teri W. Odom, Marie-Paule Pileni. *Accounts of Chemical Research* **2008** *41* (12), 1565

2. A. Paul Alivisatos. *ACS Nano* **2008** *2* (8), 1514

3. Paul S. Weiss, Penelope A. Lewis. *ACS Nano* **2008** *2* (3), 393

4. Murray, R; *Chem. Rev.* **2008,** *108,* 2688

5. M.Heaven, A. Dass, P. White, K. Holt, and Royce W. Murray. *Journal of the American Chemical Society* **2008** *130* (12), 3754

6. Christopher Love, Lara A. Estroff, Jennah K. Kriebel,,Ralph G. Nuzzo, and, George M. Whitesides. *Chemical Reviews* **2005** *105* (4), 1103

7. Teri Wang Odom, Jin-Lin Huang, Philip Kim, and Charles M. Lieber. *The Journal of Physical Chemistry B* **2000** *104* (13), 2794

8. Jesse D. Fowler, Matthew J. Allen, Vincent C. Tung, Yang Yang, Richard B. Kaner, Bruce H. Weiller. *ACS Nano* **2009** *3* (2), 301

9. Boon K. Teo, and, X. H. Sun. *Chemical Reviews* **2007** *107* (5), 1454

10. Christina M. Sweeney, Warefta Hasan, Colleen L. Nehl, Teri W. Odom. *The Journal of Physical Chemistry A* **2009** *113* (16), 4265

11. Surbhi Lal, Susan E. Clare, Naomi J. Halas. *Accounts of Chemical Research* **2008** *41* (12), 1842

12. Jeffrey N. Anker, W. Paige Hall, Olga Lyandres, Nilam C. Shah, Jing Zhao & Richard P. Van Duyne. *Nature Materials* **2008**, *7,*442

13. Michelle Duval Malinsky, K. Lance Kelly, George C. Schatz, and Richard P. Van Duyne. *J. Am. Chem. Soc.*, **2001**, *123* (7), 1471

14. Chanda Ranjit Yonzon, Eunhee Jeoung, Shengli Zou, George C. Schatz, Milan Mrksich, and Richard P. Van Duyne. *J. Am. Chem. Soc.*, **2004**, *126* (39), 12669

15. Shu-Yi Lin, Yi-Ting Tsai, Chien-Chih Chen, Chia-Mei Lin, and Chun-hsien Chen. *J. Phys. Chem. B*, **2004**, *108* (7), 2134

16, Shu-Yi Lin, Chun-hsien Chen, Meng-Chieh Lin, and Hsiu-Fu Hsu. *Anal. Chem.*, **2005**, 77 (15), 4821

17. L.E. Russell, A.A. Galyean, S.M. Notte and M.C. Leopold, *Langmuir* **2007,** 23, 7466.

18 Stephanie I. Lim, and Chuan-Jian Zhong. *Acc. Chem. Res.*, **Article ASAP**

19. Chad A. Mirkin. *Inorg. Chem.*, **2000**, *39* (11), 2258

20. D.J. Tognarelli, R.B. Miller, R.R. Pompano, A.F. Loftus, D.J. Sheibley and M.C. Leopold, *Langmuir* **2005,** 21**,** 11119

21. J. Schmitt, G. Decher, W.J. Dressick, S.L. Brandow, R.E. Geer, R. Shashidhar and J.M. Calvert, Adv. Mater. 1997, 9, 61

22. Anne A. Galyean, Robert W. Day, Justin Malinowski, Kevin W. Kittredge and Michael C. Leopold. J. of Coll. and Inter. Sci. **2009**, 331, 532

23. L.E. Russell, R.R. Pompano, K.W. Kittredge and M.C. Leopold, *J. Mater. Sci.* **2007**, 42, 7100

24 R.R. Pompano, P.G. Wortley, L.M. Moatz, D.J. Tognarelli, K.W. Kittredge and M.C. Leopold, *Thin Solid Films* **2006**, *510*, 311

25 Shu-Yi Lin, Yi-Ting Tsai, Chien-Chih Chen, Chia-Mei Lin, and Chun-hsien Chen. *J. Phys. Chem. B*, **2004**, 108 (7), 2134

26. Y. Sun, B.T. Mayers and Y. Xia, *Nano Lett.* **2002**, 2, 481

27, P. Silvert, R. Herrera-Urbina and K. Tekaia-Elhsissen, *J. Mater. Chem.* **1997**, 7,293

28. D.J. Tognarelli, R.B. Miller, R.R. Pompano, A.F. Loftus, D.J. Sheibley and M.C. Leopold, *Langmuir* **2005**, 21, 11119

29 S.E. Burke and C.J. Barrett, *Biomacromolecules* **2003**, 4 , 1773.

Appendix

Figure 1: UV-vis absorbance spectrum depicting SPB's from various LSPR nanomaterials: Ag nanoparticles, Au nanoparticles, and Au nanoshells

Figure 2: Schematic of sensing mechanism for quantification of analyte based on wavelength shift of Ag Nanoparticle from refractive index change

Figure 3: Schematic of sensing mechanism for quantification of analyte based on wavelength shift of Au nanoparticles upon analyte-mediated inter-particle distance changes (from ref. 15)

Figure 4: General design of a 5L multilayer-polymer multilayer-nanoshell film attached to a glass slide. 5L refers to the 5 layers of polymer (PLL and PSS) between the nanoshell layers. The glass substrate is modified with an amine terminated silane.

Figure 5: (left) Film growth comparisons of 1L(PLL) , 3L (PLL/PSS/PLL), and 5L (PLL/PSS/PLL/PSS/PLL) multilayer-polymer multilayer-nanoparticle films. (right) Actual image of film system on a glass slide.

Figure 6: UV–Vis spectra comparing SPBs of 1L (PLL), 3L (PLL/PSS/PLL) and 5L (PLL/PSS/PLL/PSS/PLL) multilayer-polymer multilayer-nanoparticle films compared TAS-NP in solution [From ref. 22]

Figure 7: (left) Film growth comparisons of 5L (PLL/PSS/PLL/PSS/PLL) multilayer-polymer multilayer-nanoshell films. (right) Actual image of 5L multilayer-polymer multilayer-nanoshell film system on a glass slide. [From ref. 22]

Figure 8: UV–Vis spectra showing SPB of (a) NS film in solution, (b) NS film in solution after exposure to air, and (c) a solution of NSs.

Figure 9: Changes in the λ_{max} of the SPB for solutions of NPs (solid symbols) and NSs (open symbols) as a function of the alkanethiol chainlength (i.e., methylene units, n) and terminal functional groups (-CH$_3$, -OH, -COOH, 15-crown-5). Note: The error bars refer to the standard deviation of an average based on measurements of three replicates. Some points have error bars that are smaller than the marker associated with that average

Figure 10: UV–Vis spectra showing SPB of NP film (A and C) and NS films (B and D) before and after exposure to 5 mM butanethiol (top) and tetradecanethiol (bottom) ethanol solutions for 30 min followed by copious rinsing before being reimmersed in water for absorbance measurements.

Figure 11: General design of multilayer-polymer nanoshell film, highlighting the three main components

Figure 12: Substrate effects on optical response of a nanoshell. Three multilayer-polymer monolayer-NS film designs with 0(A) , 2 (B), and 4(C) polymer layers between substrate and NS monolayer with brackets denoting the continuation of film growth with n = 15.

Figure 13: Interface effects on optical response of a nanoshell. Three mulilayer-polymer monolayer-NS film designs with 1(A) , 3(B), and 5(C) polymer layers between NS monolayer and interface, with a constant distance from substrate (n = 15). Shaded figure denotes the film-solution/air interface

Figure 14: Interparticle coupling effects on optical response of nanoshell. Three mulilayer-polymer bilayer-NS film designs with 1(A) , 3(B), and 5(C) polymer layers between NS bilayers, with a constant distance from substrate (n = 15) and constant distance from interface (p = 15)